JB Journals.ASM.org

Role of the PAS Sensor Domains in the *Bacillus subtilis* Sporulation Kinase KinA

Brit Winnen,[a] Eric Anderson,[b] James L. Cole,[b] Glenn F. King,[a,c] Susan L. Rowland[c]

Institute for Molecular Bioscience[a] and School of Chemistry and Molecular Bioscience,[c] The University of Queensland, St. Lucia, Queensland, Australia; Department of Molecular and Cell Biology, University of Connecticut, Storrs, Connecticut, USA[b]

Histidine kinases are sophisticated molecular sensors that are used by bacteria to detect and respond to a multitude of environmental signals. KinA is the major histidine kinase required for initiation of sporulation upon nutrient deprivation in *Bacillus subtilis*. KinA has a large N-terminal region (residues 1 to 382) that is uniquely composed of three tandem Per-ARNT-Sim (PAS) domains that have been proposed to constitute a sensor module. To further enhance our understanding of this "sensor" region, we defined the boundaries that give rise to the minimal autonomously folded PAS domains and analyzed their homo- and heteroassociation properties using analytical ultracentrifugation, nuclear magnetic resonance (NMR) spectroscopy, and multiangle laser light scattering. We show that PAS_A self-associates very weakly, while PAS_C is primarily a monomer. In contrast, PAS_B forms a stable dimer (K_d [dissociation constant] of <10 nM), and it appears to be the main N-terminal determinant of KinA dimerization. Analysis of KinA mutants deficient for one or more PAS domains revealed a critical role for PAS_B, but not PAS_A, in autophosphorylation of KinA. Our findings suggest that dimerization of PAS_B is important for keeping the catalytic domain of KinA in a functional conformation. We use this information to propose a model for the structure of the N-terminal sensor module of KinA.

Histidine kinases (HKs) are the most ubiquitous molecular sensors used by bacteria. They work in concert with a cognate response regulator (RR) to sense and respond to a plethora of environmental stimuli, including changes in pH, light, temperature, cellular energy levels, redox state, and the presence of toxins and food (1, 2). Some HKs are essential for bacterial viability due to their role in essential cellular processes, while others are important for mediating antibiotic resistance and virulence; this has led to the idea that some HKs might be good antimicrobial targets (2–5).

HKs function by autophosphorylating on a conserved histidine residue and then transferring the resultant high-energy phosphate to a conserved aspartate residue on the RR (6, 7). The RR is usually (but not always) a transcription factor that displays altered or enhanced affinity for its cognate DNA recognition elements upon phosphorylation (1). HKs are modular, homodimeric proteins. The cytoplasmic C-terminal domain of the protein is known bioinformatically as the HisKA domain. It is always involved in dimerization, autophosphorylation, and phosphate transfer and is made up of a four-helix bundle (the dimerization and histidine phosphotransfer [DHp] domain) that carries the phosphorylatable histidine and a C-terminal catalytic domain (often termed "Cat"), which binds ATP (8–10). HisKA is preceded by an N-terminal "sensor" module that varies in length and domain complexity between different HKs (11). Most HKs are membrane bound, and the body of the sensor module is typically separated from the catalytic domain by the membrane and the membrane-spanning regions of the protein. There are several HKs, however, that are entirely cytoplasmic and others that are membrane bound with both their N-terminal sensor and C-terminal catalytic modules in the cytoplasm.

The most common cytoplasmic signaling domains are PAS domains (12, 13). These domains are found in combination with a great variety of other signaling domains in both plant and animal proteins, but in bacteria, they are almost exclusively associated with HKs. PAS domains often mediate protein-protein interactions, and this function in turn is often modulated via ligand binding to the PAS domain (14–16). PAS domains have been shown to bind a diverse array of ligands, including heme, flavins, 4-hydroxycinnamic acid, carboxylic acids, and divalent metal ions (17).

Sporulation of *Bacillus subtilis* is a major developmental step that occurs upon nutrient starvation. Whether or not the cell commits to sporulation is determined by the level of phosphorylated Spo0A, a master transcription regulator (18, 19), which in turn is governed by a complex phosphorelay (20) initiated primarily by autophosphorylation of KinA, a cytoplasmic HK. One way in which the phosphorelay is controlled is through regulation of KinA activity via a number of antikinases; these proteins include Sda and KipI, both of which block KinA autophosphorylation (21–26). There is also a causal link between the cellular level of KinA and the bacterium's sporulation status (27).

KinA is an unusual HK in that, as well as being non-membrane bound, its N-terminal sensor module is comprised of three tandem PAS domains, termed PAS_A, PAS_B, and PAS_C (13, 28). It was suggested that the sensor module of KinA detects a sporulation-specific signal that regulates the activity of the autokinase (AK) domain. Although this hypothesis cannot be discounted as a mechanism for fine-tuning of KinA function (29), it was recently shown that the sensor module is not essential for KinA activity, as

Received 22 January 2013 Accepted 11 March 2013

Published ahead of print 15 March 2013

Address correspondence to Susan L. Rowland, s.rowland1@uq.edu.au.

Supplemental material for this article may be found at http://dx.doi.org/10.1128/JB.00096-13.

doi:10.1128/JB.00096-13

TABLE 1 Plasmids and strains used in this study

Plasmid or strain	Description or genotype	Reference
Plasmids		
WT KinA (PAS_{ABC}-AK)	IPTG-regulated promoter, pET28a origin; Kan^r; His_6-KinA wild type (residues 1–606); thrombin cleavage site	22 (His_6-$KinA^{1–606}$)
$PAS_A^{1–138}$, $PAS_A^{1–117}$, $PAS_A^{11–117}$	IPTG-regulated promoter, pGEX-2T origin; Amp^r; GST-PAS_A (residues 1–138, 1–117, or 11–117); thrombin cleavage site	This study
$PAS_B^{145–264}$, $PAS_B^{145–257}$, $PAS_B^{136–255}$	IPTG-regulated promoter, pGEX-2T origin; Amp^r; GST-PAS_B (residues 145–264, 145–257, or 136–255); thrombin cleavage site	This study
PAS_C	IPTG-regulated promoter, pGEX-2T origin; Amp^r; GST-PAS_C (residues 269–382); thrombin cleavage site	This study
PAS_{BC}-AK	IPTG-regulated promoter, pGEX-2T origin; Amp^r; GST-PAS_{BC}-autokinase (residues 136–606); thrombin cleavage site	This study
PAS_C-AK	IPTG-regulated promoter, pGEX-2T origin; Amp^r; GST-PAS_C-autokinase (residues 145–606); thrombin cleavage site	This study
AK	IPTG-regulated promoter, pET28a origin; Kan^r; His_6-autokinase (residues 383–606); thrombin cleavage site	22 (His_6-$KinA^{383–606}$)
Strains		
E. coli BL21	F^- *ompT hsdSB*(r_B^- m_B^-) *gal dcm* (DE3)	35
E. coli DH5α	*fhuA2* Δ(*argF-lacZ*)*U169 phoA glnV44* ϕ80 Δ(*lacZ*)M15 *gyrA96 recA1 relA1 endA1 thi-1 hsdR17*	34

it can be substituted with a chimeric construct that supports both KinA multimer formation and host cell sporulation (30). This suggests that the N-terminal region of KinA does not have to recognize a sporulation signal in order to activate KinA and that it instead plays a largely structural role by enhancing KinA dimerization, which then allows autophosphorylation (31). In support of this, the KinA catalytic domain by itself does not drive sporulation, but it will allow sporulation when tagged with sections of the N-terminal sensor module that support multimer formation (32). Although an order of affinity for the putative PAS-PAS homodimer interactions in the KinA sensor has been proposed (32), some questions remain about how the N-terminal domain holds the catalytic domain of KinA in a functional conformation.

In this study, we examined the KinA PAS domains from a structural perspective in an attempt to better define their structural and functional roles as well as the overall architecture of KinA. We have defined the minimal autonomously folding unit of each PAS domain, determined their oligomeric state, and examined their contribution to KinA autokinase activity. Taken together, the results allow us (i) to clarify aspects of the sensor structure that have previously been unclear and (ii) to propose a model for how the KinA sensor module holds the autokinase module in a functional conformation.

MATERIALS AND METHODS

Plasmid construction, bacterial strains, and growth media. Standard procedures were used for DNA manipulation (33). Plasmids expressing wild-type KinA (residues 1 to 606) and the His autokinase (AK) module (residues 383 to 606) were gifts from K. Cunningham (22). The strains and plasmids used in this study are described in Table 1. *Escherichia coli* DH5α (34) and *E. coli* BL21(λDE3) (35) were used for cloning experiments and protein overproduction, respectively. *E. coli* strains were grown in Luria-Bertani medium and transformed by heat shock (33) with selection on plates supplemented with 100 μg/ml ampicillin (Amp) or 25 μg/ml kanamycin (Kan).

DNA for the truncation constructs PAS_A, PAS_B, PAS_C, PAS_{BC}-AK, and PAS_C-AK (where the subscript indicates which PAS domain is included) was obtained by PCR amplification using *B. subtilis* chromosomal DNA as the template. PCR products were purified, digested by using EcoRI and BamHI, and ligated into either pGEX-2T (GE Healthcare) to generate N-terminally glutathione *S*-transferase (GST)-tagged KinA constructs or pET28a (Novagen) to generate N-terminally His_6-tagged constructs. KinA expression is isopropyl-β-D-thiogalactopyranoside (IPTG) inducible in both plasmids. Each plasmid was sequenced to verify the insert sequence.

Protein production and purification. ^{15}N-labeled PAS domains were expressed and purified according to a method that we described previously for Sda (24). Unlabeled proteins were produced by using Luria broth and then purified in the same manner as the labeled proteins. Briefly, *E. coli* BL21(λDE3) cells containing expression plasmids (listed in Table 1) were grown at 37°C, and the temperature was then shifted to 18°C once the culture optical density at 600 nm (OD_{600}) reached 0.4. Protein expression was then induced with 100 μM IPTG at an OD_{600} of 1.0. Cells were harvested by centrifugation at 22 h postinduction.

His_6-tagged proteins (wild-type [WT] KinA and the AK construct) were purified by resuspending the cell pellet in equilibration buffer (250 mM NaCl, 25 mM Tris, 10 mM imidazole, 5 mM β-mercaptoethanol [pH 7.5]) and then lysing the cells by using a cell disrupter (Constant Systems TS series benchtop) operating at a constant pressure of 25 kpsi. The cell lysate was centrifuged at 30,882.8 × *g* for 45 min at 4°C to remove insoluble debris, and the supernatant was then loaded onto Ni-nitrilotriacetic acid (NTA) resin (Qiagen), which was then washed with 10 column volumes of equilibration buffer. Proteins were liberated from the His_6 tag by on-column cleavage with thrombin (150 U per liter of culture); cleavages were performed in equilibration buffer without imidazole. Removal of the His_6 tag leaves a vestigial tripeptide sequence (GSH) at the N terminus of the protein. Cleaved proteins were eluted from the column with equilibration buffer.

For constructs harboring N-terminal GST tags (i.e., PAS_{BC}-AK and PAS_C-AK), cell lysates were obtained as described above, and the supernatant from the centrifugation step was then loaded onto glutathione affinity beads (Sigma). The column was first washed with lysis buffer (12 mM NaP_i, 150 mM NaCl, 1 mM EDTA, 2 mM dithiothreitol [DTT], 0.5 mM phenylmethylsulfonyl fluoride [PMSF] [pH 7.2]) to remove nonspecifically bound proteins, and the column was then equilibrated with thrombin cleavage buffer (150 mM NaCl, 50 mM NaP_i [pH 7.5]). Proteins were liberated from the GST tag by on-column cleavage with thrombin (150 U per liter of culture). Removal of the GST tag leaves a vestigial

dipeptide sequence (GS) at the N terminus of the protein. Cleaved proteins were eluted with lysis buffer and collected in the eluate.

For autophosphorylation assays, all proteins were first desalted into phosphorylation buffer [25 mM Tris, 250 mM NaCl, 0.5 mM EDTA, 1 mM tris(2-carboxyethyl)phosphine (TCEP), 20 mM $MgCl_2$ (pH 7.5)] by using a HighPrep 26/10 desalting column (GE Healthcare). Protein purity was analyzed by using fast protein liquid chromatography (FPLC) and SDS-PAGE.

Size exclusion chromatography (SEC) and all subsequent experiments for PAS_A and PAS_B were performed by using buffer A (20 mM Tris, 200 mM NaCl, 1 mM EDTA, 1 mM TCEP, 0.1% NaN_3 [pH 7.5]), while buffer B (50 mM Tris, 100 mM NaCl, 1 mM EDTA, 10 mM TCEP, 0.1% NaN_3 [pH 7.5]) was used for PAS_C. Proteins were desalted into these buffers as required. The solubility of PAS_C was improved at lower NaCl concentrations, and the higher concentration of reducing agent in buffer B was necessary to stop PAS_C from forming a disulfide-bonded dimer. Nuclear magnetic resonance (NMR) experiments were performed with buffer C (20 mM Tris, 150 mM NaCl, 1 mM TCEP [pH 6.85]).

Multiangle laser light scattering. Multiangle laser light scattering (MALLS) was performed as described previously (24, 36), using a miniDAWN Tristar laser light scattering photometer and an Optilab DSP interferometric refractometer (both from Wyatt Technology). SEC was performed with buffer B by using a Superdex 75 HR 10/30 column (Pharmacia Biotech). All samples were injected in a final volume of 200 μl to avoid volume-related retention time artifacts. Estimates of the weight-average molecular mass (M_w) were determined by using Debye fitting; reported errors are the standard deviations (SD) of the M_w estimate.

NMR spectroscopy. Two-dimensional (2D) ^1H-^{15}N heteronuclear single-quantum coherence (HSQC) spectra were acquired at a temperature of 298 K on Varian Inova 500- and 600-MHz spectrometers using ^{15}N-labeled PAS domains (50 to 150 μM for PAS_A, 100 to 550 μM for PAS_B, and 20 to 50 μM for PAS_C), using buffers A and B. The HSQC spectra of PAS_C in buffer A and buffer B were identical at the concentrations of protein used for these experiments, but PAS_C solubility was greater at 100 mM NaCl (buffer B). Data were processed with NMRPipe (37), and spectra were analyzed by using XEASY (38).

Analytical ultracentrifugation. Analysis of PAS domains using analytical ultracentrifugation (AUC) was carried out by using buffer A with either 1 mM TCEP (PAS_A and PAS_B) or 10 mM TCEP (PAS_C). Additional AUC experiments with PAS_C were carried out by using buffer B. The following molecular masses (M) and partial specific volumes ($\bar{\nu}$) of the PAS domain constructs were calculated at 20°C from the amino acid composition using SEDNTERP (39): PAS_A, M = 13,749, $\bar{\nu}$ = 0.7424 ml/g; PAS_B, M = 13,265, $\bar{\nu}$ = 0.7351 ml/g; PAS_C, M = 13,796, $\bar{\nu}$ = 0.7432 ml/g. AUC experiments were conducted by using a Beckman XL-I ultracentrifuge using the interference optical system. Sedimentation velocity (SV) experiments were performed by using aluminum-Epon double-sector synthetic boundary centerpieces at 20°C. Initially, the sedimentation profiles were analyzed by using the time-derivative $g(s^*)$ method with DCDT+ (40) and the $c(s)$ method with Sedfit (41). Data sets at multiple loading concentrations were also globally fitted to single ideal species (PAS_B) or monomer-dimer association models (PAS_A) by using both Sedphat (42) and Sedanal (43). Weight-average sedimentation coefficients were obtained by integration of the main peak from the $c(s)$ distributions, and the resulting S_w isotherms were fit to a monomer-dimer association model using IGOR Pro. Sedimentation equilibrium (SE) measurements of PAS_A self-association were performed by using interference optics in aged, 6-channel, external-loading cells at five protein concentrations and three rotor speeds. The data were globally analyzed by using a variety of association models using HeteroAnalysis (44).

Protein autophosphorylation assays. Proteins (0.55 to 52 μM) were incubated for 15 min at room temperature in 15 μl phosphorylation buffer (25 mM Tris, 250 mM NaCl, 0.5 mM EDTA, 1 mM TCEP, 20 mM $MgCl_2$ [pH 7.5]). Phosphorylation reactions were started by addition of 1.35 μl of a radiolabeled ATP mixture (2.5 μCi [γ-^{32}P]ATP and 2.5 μM ATP) to the protein sample, which was then incubated for 45 min (or 0 to 90 min for time course experiments) at room temperature. Reactions were stopped by addition of 5 μl of 3× SDS loading buffer to the mixture, and samples were then analyzed on a 12% SDS-PAGE gel, followed by autoradiography. The intensity of phosphorylated protein bands was determined by using Quantity One software (Bio-Rad) and compared to that from WT KinA (the PAS_{ABC}-AK construct comprising residues 1 to 606 [PAS_{ABC}-AK^{1-606}]), which was always included as a concurrent control for each protein assayed.

RESULTS

Defining the N-and C-terminal boundaries for each PAS domain. Previous studies of the primary structure of the 382-residue KinA sensor module indicated that it contained three PAS domains (13). Although the structure of most PAS domains conforms to the canonical PAS fold, the minimum autonomous folding unit of a PAS domain often cannot be determined from sequence analyses alone. The domain boundaries predicted by TIGRFAM for PAS_A, PAS_B, and PAS_C are residues 1 to 123, 139 to 262, and 263 to 387, respectively, but the PROSITE, SMART, and Pfam databases all make different predictions about the N- and C-terminal boundaries of the PAS domains. Thus, our initial subcloning of these domains was guided by additional information, including known three-dimensional (3D) structures of PAS domains and the likely position of interdomain linker regions based on V8 proteolysis of KinA (45).

PAS_A. We acquired 2D ^1H-^{15}N-^{15}N HSQC spectra of several PAS_A constructs in order to assess folding and aggregation status (46). The longest construct (PAS_A^{1-138}, where the superscript indicates domain boundaries), which corresponds closely to a previously reported proteolytic fragment of KinA (45), yielded an HSQC spectrum with overall very good chemical shift dispersion. However, there were many intense peaks with random-coil chemical shift values (i.e., ^1H chemical shifts of 7.8 to 8.6 ppm), suggestive of unstructured termini and possibly other disordered regions. Moreover, these longer constructs were unstable during purification and were naturally proteolyzed into a smaller fragment that was revealed from N-terminal sequencing and mass spectrometry to correspond to PAS_A^{1-117}. V8 proteolysis of PAS_A^{1-138} also yielded a single fragment that corresponded to PAS_A^{1-117} (data not shown). The peaks in 2D HSQC spectra of both PAS_A^{1-117} and a shorter construct, PAS_A^{11-117}, had excellent chemical shift dispersion with very few intense peaks in the random coil region, indicating that each of these proteins folds autonomously into a well-ordered tertiary structure (data not shown). In each case, however, the spectra contained approximately 25 fewer peaks than expected, even though SDS-PAGE gels indicated that the proteins had not been proteolyzed. The HSQC spectrum did not change significantly, and no additional peaks were detected with changes in protein concentration, pH, or temperature or the addition of potential ligands (ATP, ADP, and GTP at several concentrations). Similar NMR results were obtained independently in another laboratory for an almost identical PAS_A^{10-117} construct (47).

An HSQC spectrum with a defined number of missing peaks is usually indicative of a protein that is undergoing interconversion between multiple states, such as monomer-dimer exchange, which generally makes the protein unsuitable for structure determination using NMR methods. Nevertheless, the NMR results indicate that residues 1 to 117 (and residues 11 to 117) of the KinA sensor module form a stable, autonomously folded domain, as

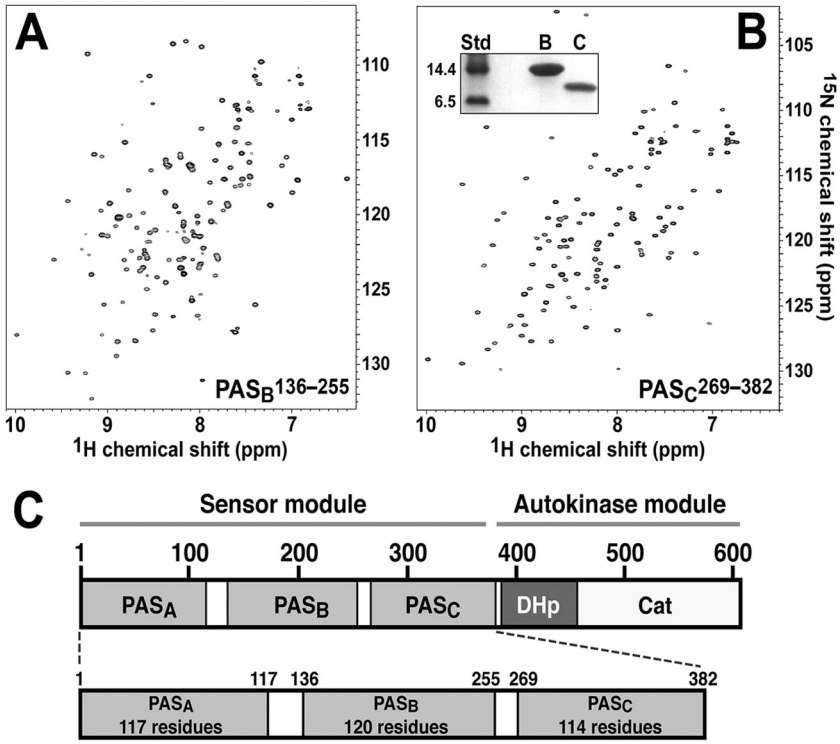

FIG 1 NMR-based analysis of the KinA sensor module. (A and B) 2D ^{1}H-^{15}N HSQC spectra of $PAS_B^{136-255}$ (A) and $PAS_C^{269-382}$ (B). The inset in panel B is a Tricine SDS-PAGE gel showing the purity of $PAS_B^{136-255}$ (lane "B") and $PAS_C^{269-382}$ (lane "C"). Std, molecular mass standards (in kDa). In each HSQC spectrum, the number of peaks observed is equivalent to the number of residues (i.e., a single resonance is observed for each backbone ^{1}H-^{15}N pair). This indicates that each domain is a monomer or a symmetric multimer. (C) Domain architecture of *B. subtilis* KinA with an expanded view of the sensor module showing the experimentally determined boundaries of the PAS domains.

reported previously by Lee and coworkers for PAS_A^{10-117} (47). Moreover, in contrast to the results obtained previously by Wang et al. (45), but consistent with the previously determined crystal structure of PAS_A^{10-117} (47), we find that this protein domain is not monomeric at concentrations above 10 μM (see below).

PAS_B. We initially subcloned a PAS_B construct that encompassed residues 145 to 264. A 2D HSQC spectrum of this construct showed a larger-than-expected variation in peak intensity, suggestive of aggregation and/or chemical exchange-induced line broadening (46). We next produced a construct with trimmed N- and C-terminal boundaries ($PAS_B^{154-257}$), which corresponds to a literature prediction for PAS_B (28). This fragment was unstable during purification and yielded an HSQC spectrum with very little chemical shift dispersion that is typical of an unfolded protein. However, a 9-residue shift of the initial PAS_B domain boundaries produced a fragment ($PAS_B^{136-255}$) that yielded a significantly improved HSQC spectrum with excellent chemical shift dispersion (Fig. 1A), indicating that this fragment autonomously folds to give a well-ordered tertiary structure. However, the peak line widths obtained for this construct were broader than those obtained for PAS_C (see below) (Fig. 1B); this might indicate that PAS_B is a dimer or undergoing a chemical exchange process that leads to NMR line broadening.

PAS_C. The HSQC spectrum of $PAS_C^{269-382}$ displayed excellent resolution (i.e., well-dispersed peaks), narrow line widths (i.e., no evidence of aggregation or other line-broadening phenomena), and minimal peak overlap (Fig. 1B). This indicates that $PAS_C^{269-382}$ is an autonomously folded monomer with very few, if any, disordered regions and is likely to be suitable for NMR structure determination.

Figure 1C shows the PAS domain boundaries as defined by the NMR analyses reported here. It is significant, as discussed further below, that these boundaries (particularly the N terminus of PAS_B) differ from those used in two previous studies where KinA domain deletion studies were performed (31, 45). A third study (32) used boundaries more similar to those which we have defined. Correct assignment of the PAS domain boundaries is critical for examining the properties of each domain.

Self-association properties of the isolated PAS domains. We used MALLS and analytical ultracentrifugation to determine the self-association properties of the purified PAS domains. For SV studies, protein samples were prepared at multiple concentrations, and data were initially analyzed to define the homogeneity of the preparations, to assess the association state(s), and to test for concentration-dependent self-association. The SV data were examined by using the time-derivative ($\partial c/\partial t$) method, a model-independent transformation of the data that enables determination of an apparent sedimentation coefficient distribution function, $g(s^*)$ (48). For PAS_B, which does not undergo reversible self-association (see below), the data were examined by using the $c(s)$ method, which models the data as a sum of noninteracting Lamm equation solutions to remove diffusional broadening (41).

PAS_A weakly self-associates. MALLS analysis of PAS_A^{1-117} (13.7 kDa) yielded a peak with a calculated M_w of 21.0 ± 0.8 kDa when the protein was loaded onto an SEC column at a concentration of 18 μM (0.25 mg/ml) (data not shown). Doubling or halv-

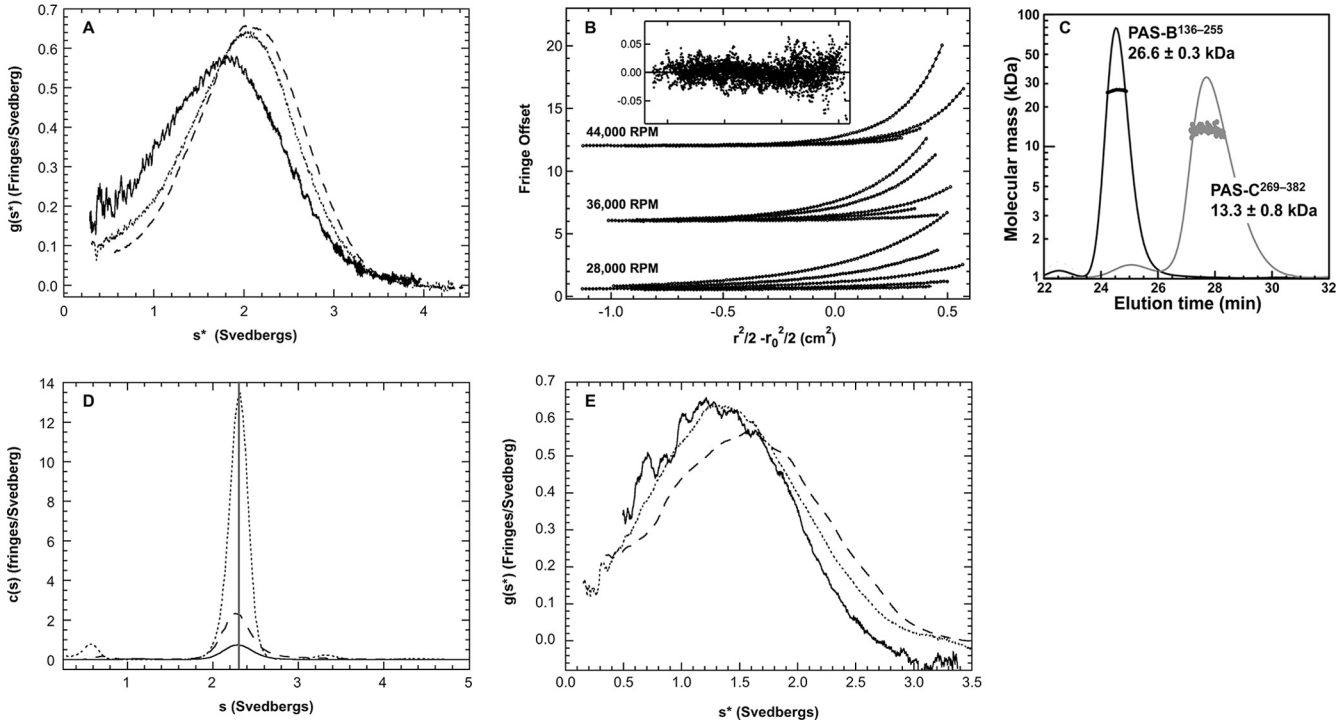

FIG 2 AUC and MALLS analysis of the N-terminal PAS domains of KinA. (A) Sedimentation velocity analysis of PAS_A. Shown are normalized $g(s^*)$ distributions obtained for PAS_A at concentrations of 0.1 mg/ml (solid), 0.6 mg/ml (dashes), and 2.0 mg/ml (dots). Conditions were as follows: rotor speed of 55,000 rpm, temperature of 20°C, and interference optics. The $g(s^*)$ distributions and weight-average sedimentation coefficients were calculated by using DCDT+ (32). (B) Sedimentation equilibrium analysis of PAS_A. Data were collected at five concentrations (0.05, 0.1, 0.2, 0.4, and 0.8 mg/ml) and three rotor speeds (28,000, 36,000, and 44,000 rpm) at 20°C using interference optics. The data are shown as points (for clarity, only every third point is shown), and the best fits are shown as lines; the inset shows the residuals. The data were globally analyzed with a monomer-dimer model using HeteroAnalysis (44) to give a best-fit K_d value 11.0 μM with an RMS deviation of 0.016 fringes. (C) PAS_B and PAS_C were fractionated on a Superdex 75 size exclusion column, and weight-average molecular masses (M_w) ± SD indicated on the chromatograms were determined by using Debye fitting (24). (D) Sedimentation velocity analysis of PAS_B. Shown are the $c(s)$ concentration distributions obtained for PAS_B at concentrations of 0.2 mg/ml (solid), 0.6 mg/ml (dashes), and 2.0 mg/ml (dots). Conditions were as follows: rotor speed of 60,000 rpm, temperature of 20°C, and interference optics. The sedimentation coefficient distribution, $c(s)$, and estimates of molecular masses were obtained by using SEDFIT (53). (E) Sedimentation velocity analysis of PAS_C. Shown are normalized $g(s^*)$ distributions obtained for PAS_C at concentrations of 0.12 mg/ml (solid), 0.6 mg/ml (dashes), and 3.0 mg/ml (dots). Conditions were as follows: rotor speed of 55,000 rpm, temperature of 20°C, and interference optics. The $g(s^*)$ distributions and weight-average sedimentation coefficients were calculated by using DCDT+ (32).

ing of this loading concentration (while maintaining the same loading volume of 100 μl) changed the M_w estimate to 22.2 ± 0.5 kDa or 19.0 ± 1.9 kDa, respectively, indicating that PAS_A undergoes a concentration-dependent self-association. Since the MALLS analysis yielded an M_w intermediate between a monomer and dimer, we conclude that PAS_A is undergoing rapid, reversible monomer-dimer exchange (although we cannot exclude the less likely possibility that the exchange is between a monomer and oligomer, with poorly populated oligomer species).

We further characterized the self-association of PAS_A using SV. Figure 2A shows the $g(s^*)$ sedimentation coefficient distributions for three concentrations of PAS_A ranging from 0.1 to 2.0 mg/ml (7.2 to 144 μM). The peak of the distribution shifts to the right with increasing PAS_A concentrations, as do the weight-average sedimentation coefficients (s_w) obtained by integration of the peaks, which increase from 1.87 S (0.1 mg/ml) to 2.14 S (2.0 mg/ml). The increase in s with increasing PAS_A concentrations indicates that the protein exists in a reversible mass action equilibrium that is rapid on the time scale of the sedimentation experiment. The SV data were globally analyzed by using a reversible monomer-dimer equilibrium model with $s_{monomer}$, s_{dimer}, and the dimer dissociation constant (K_d) as fitting parameters. Given the small range of PAS_A concentrations examined, it was necessary to fix the sedimentation coefficients to constrain the fit. Using estimates of $s_{monomer}$ of 1.5 S and s_{dimer} of 2.3 S, as reported previously for $PAS_A^{10–117}$ (47), global analysis provided an estimated K_d of 10 to 20 μM. This value is consistent with our findings from the MALLS analysis.

To further refine the K_d measurement, we rigorously characterized the behavior of PAS_A in solution using SE over a concentration range of 0.05 to 1.6 mg/ml (3.6 to 115 μM) at three rotor speeds (Fig. 2B). The data were globally analyzed by using a simple monomer-dimer model with HeteroAnalysis. A good fit was obtained, yielding a K_d of 11.0 μM (2-standard-deviation confidence interval of 9.2 to 12.9) with a root mean square (RMS) deviation of 0.016 fringes. Allowing the stoichiometry (N) to float gave a best-fit value of an N of 1.99. The fit was not further improved by allowing for thermodynamic nonideality or an incompetent monomer or dimer.

Thus, taken together, the MALLS, SV, and SE measurements convincingly demonstrate that $PAS_A^{1–117}$ exists in a weak monomer-dimer equilibrium with a K_d of ~10 μM. Thus, at the concentrations used for NMR analysis (50 to 150 μM), we would expect $PAS_A^{1–117}$ to be primarily dimeric. The absence of peaks in

the HSQC spectrum of $PAS_A^{1–117}$ is, however, suggestive of line broadening due to chemical exchange that is intermediate on the NMR time scale (46). What is this chemical exchange process if it is not interconversion between monomer and dimer? The answer is provided by the crystal structure of $PAS_A^{11–117}$, which reveals that PAS_A is capable of forming two structurally distinct dimers in which the relative orientation of the two monomeric subunits is very different (47). Thus, we conclude that the absence of peaks in the HSQC spectrum of $PAS_A^{1–117}$ is reflective of exchange between structurally distinct dimers rather than exchange between monomer and dimer.

We do not believe that the self-association of PAS_A and/or the exchange between structurally distinct dimers is physiologically relevant. The cellular concentration of KinA is very low; previous studies indicated that it varies between 0.2 μM during vegetative growth and 1.8 μM during sporulation (49). Although we cannot rule out an enhancement of dimerization affinity due to the proximity of PAS_A monomers in the context of full-length KinA, the current data suggest that PAS_A will be primarily monomeric even at the elevated KinA concentrations present during sporulation.

PAS_B is a stable dimer. Previous analyses indicated that the N-terminal region of KinA self-associates (31). Although PAS_A has the capacity to dimerize, the K_d for self-association is 10-fold higher than the physiological concentration range measured for KinA, and previous studies have shown that this self-association occurs in a nonspecific manner (47). This indicates that another region of the sensor module must be involved in KinA dimerization. Our NMR data indicated that this region is most likely PAS_B.

We initially used MALLS to analyze $PAS_B^{136–255}$ (13.8 kDa) at a very high concentration (950 μM; 13 mg/ml). We obtained a small peak with a very large M_w and a much more heavily populated peak with a calculated M_w of 26.6 ± 0.3 kDa (Fig. 2C), which is very close to the predicted size of a $PAS_B^{136–255}$ dimer (27.6 kDa). This suggests that although $PAS_B^{136–255}$ has a very slight tendency to aggregate, it is primarily a stable dimer in solution.

We used SV to further characterize the self-association of $PAS_B^{136–255}$. Figure 2D shows the $c(s)$ sedimentation coefficient distributions obtained for PAS_B over a concentration range of 0.1 to 2.0 mg/ml (7.25 to 218 μM). A major feature is observed at an s of ~2.3 S, along with a minor component at an s of 3.3 S. An additional feature at an s of ~0.5 S is likely associated with a mismatch of buffer components between the sample and reference solutions. The position of the main peak does not shift, and there is no evidence of an increasing relative contribution of the $s = 3.3$ S feature with increasing concentrations. This indicates that the peak at 2.3 S corresponds to a stable, nonequilibrating species. The higher level of S material presumably is associated with a nonequilibrating aggregate.

To define the nature of the $s = 2.3$ S species, the data at all three concentrations were globally analyzed by using a model that includes two discrete species and a continuous distribution to account for the higher-S aggregates. A good fit was obtained with RMS deviations of 0.0073 fringes and best-fit parameters for the major species of an $s_{20,w}$ of 2.41 S and an M of 27.4 kDa. The measured molecular weight is close to the predicted size of a dimer of $PAS_B^{136–255}$. Thus, over the concentration range examined, the PAS_B sample is composed of two species: an aggregate that comprises <5% of the total and a stable dimer. Based on the absence of any dissociation at the lowest concentration, we estimate that the K_d is <10 nM. Since this K_d value is 20- to 180-fold lower than the measured cellular concentrations of KinA (0.2 μM to 1.8 μM) (49), we conclude that PAS_B mediates dimerization of KinA at normal intracellular concentrations.

PAS_C is predominantly monomeric. A previous SEC analysis of a PAS_{BC} construct indicated that it dimerizes under nonreducing conditions (45). In our hands, PAS_C underwent a concentration-independent disulfide-mediated dimerization in the absence of a reducing agent, and consequently, our experiments were performed in the presence of the strong reducing agent TCEP (10 mM). MALLS analysis of PAS_C yielded a peak with an estimated M_w of 13.3 ± 0.8 kDa, consistent with a monomer (13.27 kDa) (Fig. 2C). There was also a small amount of a larger species with an elution time consistent with a dimer. The peak was too small to accurately estimate the M_w. Thus, using MALLS, we could not tell if this larger species was a residual disulfide-bonded dimer or a noncovalent dimer, so we performed AUC for clarification.

Figure 2E shows the $g(s^*)$ sedimentation coefficient distributions for $PAS_C^{269–382}$ at concentrations ranging from 0.12 to 3.0 mg/ml (9 to 226 μM) in buffer containing 200 mM NaCl. The distributions shifted slightly to higher S values at the highest concentration, and the weight-average sedimentation coefficients increased from 1.45 to 1.69 S over this concentration range, indicating that PAS_C undergoes a rapid, reversible self-association. However, the weight-average sedimentation coefficients are close to the predicted monomer value of ~1.5 S, indicating that this self-association is weak. This PAS_C self-association cannot be accurately quantified by using AUC under conditions where the oligomer is significantly populated due to complications from hydrodynamic and thermodynamic nonideality at high protein concentrations. However, if we assume that PAS_C associates to form dimers, extrapolation of our lower concentration data yields a K_d estimate of 200 to 500 μM.

Our finding that PAS_C is more soluble at lower salt concentrations led us to repeat this experiment in buffer containing 100 mM NaCl, with concentrations ranging from 0.1 to 2.0 mg/ml (7.5 to 150 μM). At the lower salt concentration, the $g(s^*)$ distributions also shifted slightly to higher S values with increasing concentrations, and the weight-average sedimentation coefficients increased from 1.45 to 1.52 S. At 100 mM NaCl, the self-association of PAS_C appeared even weaker than that at 200 mM NaCl, with a K_d of >500 μM. Thus, regardless of the salt concentration, the K_d values measured for PAS_C dimerization are >100-fold higher than the cellular concentration of KinA (49), and hence, self-association of PAS_C is unlikely to be physiologically relevant.

The PAS domains do not heteroassociate. We used NMR chemical shift mapping (46) to examine the ability of the PAS domains to associate with one another. In these experiments, we first acquired an HSQC spectrum of a ^{15}N-labeled PAS domain (PAS_A, PAS_B, or PAS_C). After this, we mixed the labeled protein sample with an unlabeled, nonself, domain preparation, and a second spectrum was acquired. All experiments were conducted under conditions where both partner proteins were soluble and folded (as indicated by the HSQC spectra). In these types of experiments, peaks are obtained for only the labeled protein. Differences in peak positions (i.e., chemical shifts) between samples with and without additional proteins are indicative of an interaction between the two proteins (46).

We observed no changes in chemical shifts or signal intensity for any of the combinations of PAS domains that we tried (^{15}N-PAS_A with PAS_B or PAS_C, ^{15}N-PAS_B with PAS_A or PAS_C, and

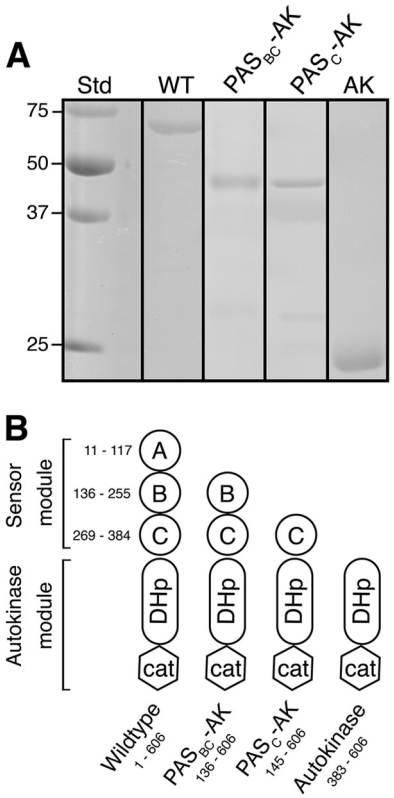

FIG 3 Production of recombinant WT KinA and KinA truncation mutants. (A) Coomassie-stained 12% SDS-PAGE gel showing purity of the purified proteins. Std, molecular mass standards (in kDa). The breakdown products seen in the PAS_{BC}-AK and PAS_C-AK lanes at ~30 kDa were reproducible. We presume that they represent the AK domain with a small amount of the PAS_C domain still attached. (B) Domain organization of WT KinA and the truncation mutants shown in panel A. The N- and C-terminal boundaries used for each of the KinA constructs are indicated.

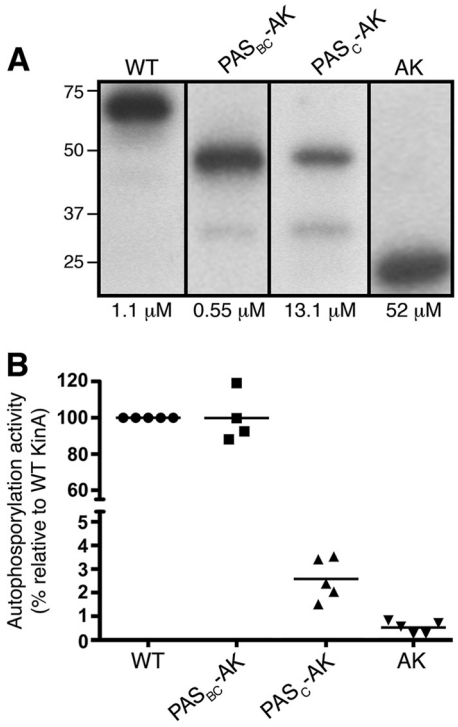

FIG 4 Autophosphorylation activity of WT KinA and KinA truncation mutants. WT KinA ($KinA^{1-606}$), PAS_{BC}-AK ($KinA^{136-606}$), PAS_C-AK ($KinA^{145-606}$), and AK ($KinA^{383-606}$) were incubated for 45 min at room temperature at different concentrations with 2.5 μCi [^{32}P]ATP and 2.5 μM ATP. Reactions were stopped by adding SDS loading buffer to the samples, and samples were analyzed on a 12% SDS-PAGE gel, followed by autoradiography. (A) Autoradiogram of WT KinA and truncation mutants. The protein concentration in each assay mixture is given in μM. The same volume of assay mixture was loaded into each lane. Std, molecular mass standards (in kDa). (B) Quantification of phosphorylation activity. The five values are from five independent assays in each case. Bars indicate mean values. WT KinA activity was set at 100%.

^{15}N-PAS_C with PAS_B or PAS_A). Although we cannot rule out a role for (i) proximity due to tethering or (ii) accessory factors in driving PAS domain interactions in intact KinA, our results suggest that there is no heterodomain interactions between PAS_A, PAS_B, and PAS_C.

Role of the PAS domains in KinA autophosphorylation. In order to examine the influence of each PAS domain on KinA autokinase activity, we constructed a series of truncated KinA proteins in which each of the three PAS domains was removed stepwise, as shown in Fig. 3B. The NMR data were used to determine the domain boundaries for each construct. SDS-PAGE analysis revealed purity greater than 90% for all constructs (Fig. 3A), and the apparent molecular masses were close to the predicted values (WT = 69.4 kDa; PAS_{BC}-AK = 53.7 kDa; PAS_C-AK = 52.7 kDa; AK = 25.1 kDa).

Autophosphorylation of full-length WT KinA was measured via the incorporation of radioactivity into KinA upon incubation with [γ-^{32}P]ATP. Samples were electrophoresed by using SDS-PAGE, and phosphorylated KinA was then visualized by using autoradiography (Fig. 4A). Autophosphorylation of WT KinA reached a maximum after 90 min of incubation under the chosen experimental conditions (data not shown), and a comparison of the extent of autophosphorylation of WT KinA and the various truncation constructs over this time period is shown in Fig. 4A. The intensities of phosphorylated protein on the autoradiogram were quantified by using the Quantity One program, and mean values are shown in Fig. 4B. The autokinase activity of WT KinA was set at 100%. Deletion of PAS_A had little effect on autokinase activity, as the PAS_{BC}-AK construct showed only a small decrease in autophosphorylation (92% relative to that of WT KinA).

As mentioned above, we initially subcloned a PAS_B domain that started at residue 145 (since domain boundary predictions by several bioinformatics programs were inconclusive). However, our NMR data revealed that a fully folded and stable PAS_B domain requires residues 136 to 145. Consequently, we conclude that the PAS_{BC}-AK construct comprising residues 145 to 606 contains an incomplete PAS_B domain that is likely partially unfolded and highly flexible at the N terminus, and hence, we have renamed this construct PAS_C-AK. Interestingly, the autophosphorylation ability of this protein is almost abolished; it shows only 2.5% activity compared to that of WT KinA (Fig. 4B), indicating that a fully folded PAS_B domain is required for kinase activity. These *in vitro* data are consistent with previously reported *in vivo* observations that (i) the PAS_C domain alone does not support sporulation and (ii) in experimental situations, the PAS_B domain is required for sporulation (32). Since it appears that PAS_B is critical for autophosphorylation of KinA, it was not surprising that the AK con-

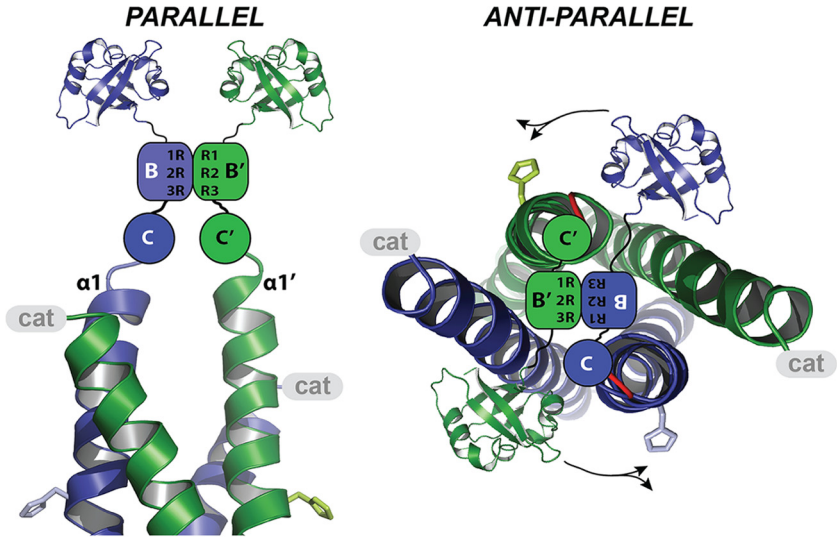

FIG 5 Models for possible conformations of the KinA sensor dimer. The DHp and PAS_A domain structures are shown as Richardson representations, with monomers indicated by color (blue and green) and the inclusion of a prime. Structure coordinates were taken from data reported under Protein Data Bank (PDB) accession numbers 3DGE (DHp from *Thermotoga maritima* [7]) and 2VLG (PAS_A from *B. subtilis* [47]). The dimeric structure is consistent with data for native, nontagged KinA reported previously by Lee et al. (47). (A) Sensor arrangement with PAS_B in a parallel dimer configuration. R1, R2, and R3 designate three side chains so that the viewer can orient the structure and examine the symmetry of the dimer. (B) Sensor arrangement with PAS_B in the antiparallel dimer configuration (top view, looking down on the DHp four-helix bundle). In this arrangement, the PAS_B domains lies "flat" across the end of the DHp domain. In the two configurations shown here, each monomer in the dimer experiences the same twisting forces. B and C, PAS_B and PAS_C, respectively; α1, N terminus of DHp helix 1; black line, peptide backbone of the protein; cat, catalytic ATP-binding domain. Two-headed arrows indicate the movements that may lead to HK activation and deactivation. These are (i) 26° helical rotations of α2 against α1, as shown previously for EnvZ by Ferris et al. (52), and (ii) "helix cracking" in α2 proposed previously for KinA by Dago et al. (51).

struct, in which the entire sensor module had been removed, showed very limited autophosphorylation (1% of the activity of WT KinA) (Fig. 4B). To detect autophosphorylation of this construct, very high protein concentrations had to be used (52 μM) (Fig. 4A). The observations reported here are consistent with previously reported *in vivo* data showing that the AK domain alone is not able to induce sporulation in *B. subtilis* (32).

DISCUSSION

Phosphorylation of KinA (and, to a lesser extent, KinB, KinC, and KinD [50]) is the initial step required to activate the multicomponent phosphorelay that controls sporulation in *B. subtilis*. The regulation of KinA is therefore critical to ensure that bacteria switch to the irreversible stages of sporulation only under severely nutrient-deprived conditions. The N-terminal sensor module (or another protein sequence that supports KinA multimerization) is essential for the activity of KinA (30, 45). However, despite numerous efforts, much remains to be learned about how the sensor module influences and regulates KinA. Some information exists about how the N-terminal sensor module holds the catalytic domain of KinA in a functional conformation, but interpretation of the existing data is difficult due to the use of different PAS domain boundaries in various protein constructs.

We used a combination of biochemical and biophysical approaches in order to (i) examine the structural features of the individual PAS domains, (ii) carefully define their functional boundaries, and (iii) elucidate their roles in KinA autophosphorylation. NMR and AUC experiments indicated that PAS_B is the only PAS domain in the KinA sensor module that can form a stable dimer at physiologically relevant concentrations. We demonstrated that, in the context of native KinA, the autokinase activity of the protein is critically dependent on PAS_B but that PAS_A is dispensable. We suggest that the primary role of PAS_C is structural: it links PAS_B and the AK domain in the correct orientation to allow both ends of the monomer to dimerize effectively.

The data presented here are to some extent consistent with results reported previously by Wang et al. (45), who showed that the sensor module of KinA is critical for kinase activity, with deletion of all three PAS domains abolishing autophosphorylation. In contrast to our findings, however, Wang and coworkers observed that deletion of PAS_A caused a >90% reduction in autophosphorylation activity; they concluded that PAS_A is essential for efficient autokinase activity. Similarly, Lee and colleagues (47) concluded that deletion of PAS_A significantly diminished KinA activity, as measured indirectly via a green fluorescent protein (GFP) reporter assay of sporulation pathway activation. These contrary observations may be due to the different domain boundaries chosen to construct truncated KinA proteins: the "PAS_A deletion" construct used by Wang et al. (45) lacks residues 136 to 143 of the PAS_B domain that we have defined and shown here to be critical for KinA autophosphorylation, while the construct used by Lee et al. (47) lacks PAS_B residues 136 to 151. Our results are consistent with recent *in vivo* functional studies showing that KinA with a deletion of residues 1 to 136 (which deletes PAS_A completely but leaves the PAS_B domain intact) induced sporulation at wild-type levels irrespective of nutrient availability (31).

Symmetric model of the sensor domain. Our findings allow us to propose a model for the dimeric KinA sensor module in which the two monomers align in a symmetric fashion (Fig. 5), with PAS_B comprising the core of the dimeric structure. This configuration is consistent with the HSQC spectrum obtained for PAS_B, which has the requisite number of backbone peaks for a

protein of the size of PAS_B but displays line-broadening characteristic of a dimer. The peak count indicates that only a single chemical state exists for each of the backbone amide protons, suggesting that PAS_B exists as a symmetric dimer. An asymmetric configuration of the dimer would expose each residue to two different environments, and thus, each ^{1}H-^{15}N pair would generate two HSQC peaks, which is not what we observed. It should be noted that a symmetric dimer can be achieved in two ways (Fig. 5), via a parallel or antiparallel alignment. In the parallel arrangement (Fig. 5A), the PAS_B dimer would most likely protrude vertically from the end surface of the DHp domain. In the antiparallel arrangement (Fig. 5B), the PAS_B dimer can lie flat across the end surface of the four helices of the DHp domain. Our data do not allow us to discriminate between these two possible conformations.

An interesting prediction of the sensor domain model is the position of PAS_C and its role in linking PAS_B with the AK module. Presumably, the relative orientation of PAS_B and PAS_C must be important, and homology searches reinforce this point. There are currently 31 records in UniProt for KinA homologues with all three PAS domains in the N-terminal region (search conducted on 16 January 2013). Figure S1 in the supplemental material shows an alignment of a subset of these proteins, one from each representative species from the BLAST results. This alignment reveals an extraordinary level of conservation of the entire region from the beginning of PAS_B to the phosphorylatable His405 in the DHp domain of KinA. In this region of KinA, PAS_B is actually the least conserved region (72% similarity across all homologues); in contrast, PAS_C is 83% conserved, and quite remarkably, the PAS_{BC} linker is 100% conserved. In contrast, the PAS_{AB} linker is very divergent between homologues (only 5.5% conservation), while PAS_A itself also shows more moderate conservation (67%). It is interesting to note that residues 351 to 513 are 100% conserved between homologues: this region neatly spans the C-terminal region of PAS_C, the beginning of helix 1 in the KinA DHp domain, and the crucial His405 residue.

Clearly, this region of KinA is functionally important, but how does the sensor module regulate KinA activity and thereby control sporulation? It has been suggested that KinA might be regulated by starvation-associated intracellular ligands that, upon recognition by the sensor module, would activate autophosphorylation of KinA. This idea is controversial. Unstarved vegetative cells can sporulate at wild-type levels if they are artificially induced to produce sporulation-associated levels of KinA (49). This suggests that KinA activity is not downregulated to any significant degree by environmental signals and that instead it is "on" all the time (30).

Recently, however, Dago et al. (51) presented molecular dynamics (MD) simulations and bioinformatic evidence for discrete sets of stabilizing interdomain contacts in KinA that are consistent with two states. In the "on" state, the ATP-binding pocket of the Cat domain has access to the phosphorylatable histidine in the DHp domain, while in the "off" state, it is sequestered away from His405. Those authors posited that the transition between these two states is driven by ligand binding to the sensor region. Using NMR and X-ray crystallographic structures of HKs locked in the active and inactive configurations, Ferris et al. (52) also showed that maintenance of the off state of an HK involves sequestration of the Cat domain by a small set of conserved interdomain interactions. Interestingly, both groups showed that the transition between the on and off conformations involves movements at the "top" or sensor-proximal ends of the DHp domain helices and not at the phosphorylatable histidine itself. The MD simulations performed by Dago et al. (51) indicate that in KinA, these movements occur at the C-terminal end of DHp helix 2 (directly N terminal to the DHp-Cat linker), while helix 1 remains relatively static.

Our work does not exclude either the static "on" model of KinA or the model in which KinA switches between two states through sensor-ligand interactions. Our proposed sensor arrangement tethers the N-terminal regions of the DHp helix 1 pair near one another, but it does not necessarily affect the orientation or location of helix 2. It is possible that PAS_A and PAS_C can flex and that, in doing so, they interact variably with helix 1, helix 2, or the Cat domain. This may provide a mechanism for KinA regulation. In contrast, PAS_B is a tight dimer and is unlikely to be a modulator of KinA activity; instead, it helps maintain KinA in a conformation where it is able to function as a dimer and autophosphorylate.

ACKNOWLEDGMENTS

We thank Katie Cunningham and Bill Burkholder for the gifts of plasmids described in the text.

B.W. is a recipient of the Feodor Lynen Research Fellowship from the Alexander von Humboldt Foundation. We acknowledge funding from the Australian National Health and Medical Research Council (project grant APP1010776 to G.F.K.) and The University of Queensland (UQ early career researcher grant to S.L.R.).

REFERENCES

1. **Stock AM, Robinson VL, Goudreau PN.** 2000. Two-component signal transduction. Annu. Rev. Biochem. **69**:183–215.
2. **Rowland SL, King GF.** 2007. Histidine kinases as antimicrobial targets: prospects and pitfalls. Mini Rev. Med. Chem. **7**:1144–1154.
3. **Gotoh Y, Eguchi Y, Watanabe T, Okamoto S, Doi A, Utsumi R.** 2010. Two-component signal transduction as potential drug targets in pathogenic bacteria. Curr. Opin. Microbiol. **13**:232–239.
4. **Stephenson K, Hoch JA.** 2004. Developing inhibitors to selectively target two-component and phosphorelay signal transduction systems of pathogenic microorganisms. Curr. Med. Chem. **11**:765–773.
5. **Okada A, Gotoh Y, Watanabe T, Furuta E, Yamamoto K, Utsumi R.** 2007. Targeting two-component signal transduction: a novel drug discovery system. Methods Enzymol. **422**:386–395.
6. **Casino P, Rubio V, Marina A.** 2010. The mechanism of signal transduction by two-component systems. Curr. Opin. Struct. Biol. **20**:763–771.
7. **Casino P, Rubio V, Marina A.** 2009. Structural insight into partner specificity and phosphoryl transfer in two-component signal transduction. Cell **139**:325–336.
8. **Tomomori C, Tanaka T, Dutta R, Park H, Saha SK, Zhu Y, Ishima R, Liu D, Tong KI, Kurokawa H, Qian H, Inouye M, Ikura M.** 1999. Solution structure of the homodimeric core domain of *Escherichia coli* histidine kinase EnvZ. Nat. Struct. Biol. **6**:729–734.
9. **Tanaka T, Saha SK, Tomomori C, Ishima R, Liu D, Tong KI, Park H, Dutta R, Qin L, Swindells MB, Yamazaki T, Ono AM, Kainosho M, Inouye M, Ikura M.** 1998. NMR structure of the histidine kinase domain of the *E. coli* osmosensor EnvZ. Nature **396**:88–92.
10. **Wolanin PM, Thomason PA, Stock JB.** 2002. Histidine protein kinases: key signal transducers outside the animal kingdom. Genome Biol. **3**:REVIEWS3013. doi:10.1186/gb-2002-3-10-reviews3013.
11. **Mascher T, Helmann JD, Unden G.** 2006. Stimulus perception in bacterial signal-transducing histidine kinases. Microbiol. Mol. Biol. Rev. **70**:910–938.
12. **Galperin MY.** 2004. Bacterial signal transduction network in a genomic perspective. Environ. Microbiol. **6**:552–567.
13. **Taylor BL, Zhulin IB.** 1999. PAS domains: internal sensors of oxygen, redox potential, and light. Microbiol. Mol. Biol. Rev. **63**:479–506.
14. **Gilles-Gonzalez MA, Gonzalez G.** 2004. Signal transduction by heme-containing PAS-domain proteins. J. Appl. Physiol. **96**:774–783.
15. **Lindebro MC, Poellinger L, Whitelaw ML.** 1995. Protein-protein inter-

action via PAS domains: role of the PAS domain in positive and negative regulation of the bHLH/PAS dioxin receptor-Arnt transcription factor complex. EMBO J. **14**:3528–3539.
16. **Scheuermann TH, Tomchick DR, Machius M, Guo Y, Bruick RK, Gardner KH.** 2009. Artificial ligand binding within the HIF2alpha PAS-B domain of the HIF2 transcription factor. Proc. Natl. Acad. Sci. U. S. A. **106**:450–455.
17. **Henry JT, Crosson S.** 2011. Ligand-binding PAS domains in a genomic, cellular, and structural context. Annu. Rev. Microbiol. **65**:261–286.
18. **Fawcett P, Eichenberger P, Losick R, Youngman P.** 2000. The transcriptional profile of early to middle sporulation in *Bacillus subtilis*. Proc. Natl. Acad. Sci. U. S. A. **97**:8063–8068.
19. **Molle V, Fujita M, Jensen ST, Eichenberger P, Gonzalez-Pastor JE, Liu JS, Losick R.** 2003. The Spo0A regulon of Bacillus subtilis. Mol. Microbiol. **50**:1683–1701.
20. **Burbulys D, Trach KA, Hoch JA.** 1991. Initiation of sporulation in *B. subtilis* is controlled by a multicomponent phosphorelay. Cell **64**:545–552.
21. **Burkholder WF, Kurtser I, Grossman AD.** 2001. Replication initiation proteins regulate a developmental checkpoint in *Bacillus subtilis*. Cell **104**: 269–279.
22. **Cunningham KA, Burkholder WF.** 2009. The histidine kinase inhibitor Sda binds near the site of autophosphorylation and may sterically hinder autophosphorylation and phosphotransfer to Spo0F. Mol. Microbiol. **71**: 659–677.
23. **Jacques DA, Langley DB, Jeffries CM, Cunningham KA, Burkholder WF, Guss JM, Trewhella J.** 2008. Histidine kinase regulation by a cyclophilin-like inhibitor. J. Mol. Biol. **384**:422–435.
24. **Rowland SL, Burkholder WF, Cunningham KA, Maciejewski MW, Grossman AD, King GF.** 2004. Structure and mechanism of action of Sda, an inhibitor of the histidine kinases that regulate initiation of sporulation in *Bacillus subtilis*. Mol. Cell **13**:689–701.
25. **Wang L, Grau R, Perego M, Hoch JA.** 1997. A novel histidine kinase inhibitor regulating development in *Bacillus subtilis*. Genes Dev. **11**:2569–2579.
26. **Whitten AE, Jacques DA, Hammouda B, Hanley T, King GF, Guss JM, Trewhella J, Langley DB.** 2007. The structure of the KinA-Sda complex suggests an allosteric mechanism of histidine kinase inhibition. J. Mol. Biol. **368**:407–420.
27. **Eswaramoorthy P, Dinh J, Duan D, Igoshin OA, Fujita M.** 2010. Single-cell measurement of the levels and distributions of the phosphorelay components in a population of sporulating *Bacillus subtilis* cells. Microbiology **156**:2294–2304.
28. **Stephenson K, Hoch JA.** 2001. PAS-A domain of phosphorelay sensor kinase A: a catalytic ATP-binding domain involved in the initiation of development in *Bacillus subtilis*. Proc. Natl. Acad. Sci. U. S. A. **98**:15251–15256.
29. **McLoon AL, Kolodkin-Gal I, Rubinstein SM, Kolter R, Losick R.** 2011. Spatial regulation of histidine kinases governing biofilm formation in *Bacillus subtilis*. J. Bacteriol. **193**:679–685.
30. **Eswaramoorthy P, Dravis A, Devi SN, Vishnoi M, Dao HA, Fujita M.** 2011. Expression level of a chimeric kinase governs entry into sporulation in *Bacillus subtilis*. J. Bacteriol. **193**:6113–6122.
31. **Eswaramoorthy P, Guo T, Fujita M.** 2009. In vivo domain-based functional analysis of the major sporulation sensor kinase, KinA, in *Bacillus subtilis*. J. Bacteriol. **191**:5358–5368.
32. **Eswaramoorthy P, Fujita M.** 2010. Systematic domain deletion analysis of the major sporulation kinase in *Bacillus subtilis*. J. Bacteriol. **192**:1744–1748.
33. **Sambrook J, Fritsch EF, Maniatis T.** 1989. Molecular cloning: a laboratory manual, 2nd ed. Cold Spring Harbor Laboratory Press, Cold Spring Harbor, NY.
34. **Taylor RG, Walker DC, McInnes RR.** 1993. *E. coli* host strains significantly affect the quality of small scale plasmid DNA preparations used for sequencing. Nucleic Acids Res. **21**:1677–1678.
35. **Studier FW, Moffatt BA.** 1986. Use of bacteriophage T7 RNA polymerase to direct selective high-level expression of cloned genes. J. Mol. Biol. **189**: 113–130.
36. **Folta-Stogniew E, Williams KR.** 1999. Determination of molecular masses of proteins in solution: implementation of an HPLC size exclusion chromatography and laser light scattering service in a core laboratory. J. Biomol. Tech. **10**:51–63.
37. **Delaglio F, Grzesiek S, Vuister GW, Zhu G, Pfeifer J, Bax A.** 1995. NMRPipe: a multidimensional spectral processing system based on UNIX pipes. J. Biomol. NMR **6**:277–293.
38. **Bartels C, Xia T, Billeter M, Güntert P, Wüthrich K.** 1995. The program XEASY for computer-supported NMR spectral analysis of biological macromolecules. J. Biomol. NMR **6**:1–10.
39. **Laue TM, Shah BD, Ridgeway TM, Pelletier SL.** 1992. Computer-aided interpretation of analytical sedimentation data for proteins, p 90–125. *In* Harding SE, Rowe AJ, Horton JC (ed), Analytical ultracentrifugation in biochemistry and polymer science. Royal Society of Chemistry, Cambridge, United Kingdom.
40. **Philo JS.** 2000. A method for directly fitting the time derivative of sedimentation velocity data and an alternative algorithm for calculating sedimentation coefficient distribution functions. Anal. Biochem. **279**:151–163.
41. **Schuck P.** 2000. Size-distribution analysis of macromolecules by sedimentation velocity ultracentrifugation and Lamm equation modeling. Biophys. J. **78**:1606–1619.
42. **Schuck P.** 2003. On the analysis of protein self-association by sedimentation velocity analytical ultracentrifugation. Anal. Biochem. **320**:104–124.
43. **Stafford WF, Sherwood PJ.** 2004. Analysis of heterologous interacting systems by sedimentation velocity: curve fitting algorithms for estimation of sedimentation coefficients, equilibrium and kinetic constants. Biophys. Chem. **108**:231–243.
44. **Cole JL.** 2004. Analysis of heterogeneous interactions. Methods Enzymol. **384**:212–232.
45. **Wang L, Fabret C, Kanamaru K, Stephenson K, Dartois V, Perego M, Hoch JA.** 2001. Dissection of the functional and structural domains of phosphorelay histidine kinase A of *Bacillus subtilis*. J. Bacteriol. **183**:2795–2802.
46. **Bieri M, Kwan AH, Mobli M, King GF, Mackay JP, Gooley PR.** 2011. Macromolecular NMR spectroscopy for the non-spectroscopist: beyond macromolecular solution structure determination. FEBS J. **278**:704–715.
47. **Lee J, Tomchick DR, Brautigam CA, Machius M, Kort R, Hellingwerf KJ, Gardner KH.** 2008. Changes at the KinA PAS-A dimerization interface influence histidine kinase function. Biochemistry **47**:4051–4064.
48. **Stafford WF, III.** 1992. Boundary analysis in sedimentation transport experiments: a procedure for obtaining sedimentation coefficient distributions using the time derivative of the concentration profile. Anal. Biochem. **203**:295–301.
49. **Eswaramoorthy P, Duan D, Dinh J, Dravis A, Devi SN, Fujita M.** 2010. The threshold level of the sensor histidine kinase KinA governs entry into sporulation in *Bacillus subtilis*. J. Bacteriol. **192**:3870–3882.
50. **Jiang M, Shao W, Perego M, Hoch JA.** 2000. Multiple histidine kinases regulate entry into stationary phase and sporulation in *Bacillus subtilis*. Mol. Microbiol. **38**:535–542.
51. **Dago AE, Schug A, Procaccini A, Hoch JA, Weigt M, Szurmant H.** 2012. Structural basis of histidine kinase autophosphorylation deduced by integrating genomics, molecular dynamics, and mutagenesis. Proc. Natl. Acad. Sci. U. S. A. **109**:E1733–E1742. doi:10.1073/pnas.1201301109.
52. **Ferris HU, Dunin-Horkawicz S, Hornig N, Hulko M, Martin J, Schultz JE, Zeth K, Lupas AN, Coles M.** 2012. Mechanism of regulation of receptor histidine kinases. Structure **20**:56–66.
53. **Schuck P, Perugini MA, Gonzales NR, Howlett GJ, Schubert D.** 2002. Size-distribution analysis of proteins by analytical ultracentrifugation: strategies and application to model systems. Biophys. J. **82**:1096–1111.